Neutrinos from the Cosmic Noon

Riya[1] and Vikram Rentala[2]

[1]*Department of Mechanical Engineering, Indian Institute of Technology Bombay, Powai, Mumbai 400076, India**
[2]*Department of Physics, Indian Institute of Technology Bombay, Powai, Mumbai 400076, India*†

Multiple astrophysical probes of the star formation rate (SFR) yield widely different inferences of this rate at redshifts greater than 1. While all probes seem to indicate a period of peak star formation known as cosmic noon, the detailed inferences from these probes are in disagreement. The peak indicated by the UV/IR data is significantly lower than the peak indicated by Hα data. In this work, the potential of measurement of the diffuse supernova neutrino background (DSNB) at HyperKamiokande, is explored, to resolve the discrepancy and help pin down the magnitude of peak star formation.

INTRODUCTION

Galaxies are the systems that dictate the evolution of baryons in the universe. To understand the fate of all the matter in the universe, understanding the origin and evolution of galaxies is unavoidable. The evolution of cosmic star formation rate density is one of the critical components required to describe galaxy evolution. Most of the observations indicate a peak in the global star formation rate (SFR) between redshift 1 and 3, indicating it to be the epoch of most vigorous star formation [11]. This redshift range is known as the cosmic noon. It is speculated that half of the mass of the universe today was formed during cosmic noon [13]. That is the reason why the study of cosmic noon is so exciting.

However, there are many challenges in the path. There is no theory which can predict at which redshift the peak is or what is its magnitude and therefore we need to rely on observations to get this information. While the observations in different wavelength region have shown the epoch to lie in the redshift range mentioned above, the SFR density over this range remains uncertain. In this paper, current probes used to measure the star formation rate and their limitations, along with the discrepancies in star formation rate obtained from different probes, are discussed. We propose to measure star formation rate using diffused supernova neutrino background (DSNB). The majority of the paper is devoted to the analysis of the capacity of DSNB measurements, from existing and proposed experiments, to validate a given global star formation rate. Throughout this paper, we use values of cosmological parameters: $\Omega_m = 0.3$, $\Omega_\Lambda = 0.7$, $\Omega_r = 0.4956 \times 10^{-5}$ and $H_0 = 71$ kms^{-1}Mpc^{-1}[11].

PROBES OF STAR FORMATION HISTORY

In the star formation rate measurement, mass is inferred from light. This conversion requires knowledge of mass to light ratio, which depends on age, star-formation history, and extinction due to dust. Currently, this ratio is obtained using population synthesis models which compute the predicted spectrum of a galaxy. Synthesis models evaluate evolutionary tracks, i.e., how luminosity, temperature and radius vary as functions of mass and age and add stellar atmosphere to find spectra of stars. Isochrone spectrum is obtained by summing the spectra over IMF, whose sum over a chosen star formation history gives the current spectrum. Integrated light, which is only observable quantity, is used to determine the properties of galaxies (needed as input in the model). However, various properties such as age, metallicity and dust attenuation, affect the integrated light making the determination of individual properties uncertain. Therefore, the whole process is error-prone. [14] [10]

Due to the above reasons, the star formation rate, as estimated through different probes, differ significantly. The situation worsens for high redshift, where the number of probes is limited, and the uncertainty in measurement is significant. Commonly used probes to measure the star formation rate, along with their advantages and weakness, are listed below.

- **Ultraviolet rays (referred to as UV henceforth)**
  - **Principle** UV rays are emitted by massive stars which have short lifetimes. Therefore, UV emission dominates the luminosity in a young simple stellar population (SSP) but fades quickly as an SSP ages. Consequently, the luminosity of UV rays is correlated to SFR.
  - **Benefits**
    - Applicable for a broad range of redshifts (1.4 to 6) [9]
    - Very sensitive, i.e., can measure moderate SFRs also. (SFR of $\sim 10^{-4}$ $M_\odot$ yr^{-1} has been measured using UV rays. [8])
  - **Shortcomings**
    - The sensitivity of estimated SFR to assumed IMF, dust-correction and metallicity values

- **Far Infrared Rays (referred to as IR henceforth)**
  - **Principle** Dust absorbs energy from the UV and re-radiates the energy at IR wavelengths.
  - **Benefits**
    * Negligible dust absorption
  - **Shortcomings**
    * Difficulty in distinguishing infrared rays from star formation processes and infrared rays from dust warmed by older stellar population or active nuclei
    * The sensitivity of estimated SFR to the very complex dust emission spectrum
- **Hα**
  - **Principle** UV rays ionizes hydrogen atoms. Hα is one of the resulting recombination lines.
  - **Benefits**
    * Very sensitive, i.e., can measure moderate SFRs also. (SFR of $\sim 10^{-5}$ $M_\odot$ yr^{-1} has been measured using UV rays. [8])
    * Direct measurement of SFR (not dependent on interstellar medium (ISM) conditions)
    * High spatial resolution (Full Width at Half Maximum (FWHM) $\sim$ 2.5 arcsec)
  - **Shortcomings**
    * Can be absorbed by dust grains
    * Overestimated values due to the presence of active galactic nuclei
- **Radio emission**
  - **Principle** Ionized gas radiates at high-frequency radio wavelengths. Lower frequencies are emitted by diffuse cosmic rays generated in supernova shocks. Despite the indirect link of low frequencies radio to SFR, a tight correlation is observed between radio emission and FIR emission in local galaxies.
  - **Benefits**
    * Free from dust extinction
    * Independent of redshift (no reddening) [14]
  - **Shortcomings**
    * Difficulty in distinguishing radio emission from star formation processes and radio emission from active galactic nuclei
    * Hard to calibrate because of the uncertainties of SNR and CR production and the uncertainties in synchrotron efficiencies

DISCREPANCIES IN STAR FORMATION RATE

In Madau and Dickinson, observed UV and IR Star Formation Rate Densities (SFRDs) are obtained analyzing the data from surveys that have measured SFRs from rest-frame far-UV or mid-infrared and far-infrared measurements. Co-moving luminosity densities have been obtained integrating luminosity functions given in the surveys, which are then multiplied with the conversion factors to obtain observed SFRDs. The SFRDs measured using UV is then corrected for dust attenuation using an effective dust extinction. The SFRs obtained from UV after dust correction agrees with the SFRs obtained from IR. Best-fitting function for the SFRDs is obtained as:

$$R_{SF}(z) = 0.015\frac{(1+z)^{2.7}}{1+\left[\frac{(1+z)}{2.9}\right]^{5.6}}\ M_\odot\ \text{year}^{-1}\ \text{Mpc}^{-3} \quad (1)$$

We want to compare this SFR with the one obtained using Hα. Radio emissions are not considered in this work because of comparatively limited and indirect information provided by it. It is decided to have the same form of the fitting function to have a better comparison, and both types of data are fitted by tuning the parameters. The following fitting function is used for the purpose (referred to as Shunsaku fitting function henceforth) [7].

$$R_{SF}(z) = \rho\left[(1+z)^{\alpha\eta} + \left(\frac{1+z}{B}\right)^{\beta\eta} + \left(\frac{1+z}{C}\right)^{\gamma\eta}\right]^{1/\eta} \quad (2)$$

where R_{SF}(z) represents the total mass of stars formed per unit coordinate volume per unit time and

$$B = (1+z_1)^{1-\alpha/\beta} \quad (3)$$

$$C = (1+z_1)^{(\beta-\alpha)/\gamma}(1+z_2)^{1-\beta/\gamma} \quad (4)$$

100 SFR values are generated between redshift 0 and 10 using equation 1 which are fitted in Shunsaku fitting function (equation 2), to get the parameter values for the UV and IR data: $\rho = 0.015$, $\alpha = 2.7$, η = -1, $z_1 = 2.2$, β = -2.9, γ = -2.9, $z_2 = 21.8$

To get the parameter values for the Hα data, SFR values from [11] and [12] was used. The value of parameters obtained on using Shunsaku fitting function: $\rho = 0.007$, $\alpha = 4.5$, η = -90.2, $z_1 = 2.3$, $\beta = 1$, γ = -2.9, $z_2 = 3.5$

Both the fits are shown in figure 1. It can be seen from the plot that the peak SFR predicted from Hα data is approximately four times larger than the one predicted by UV and IR data. This discrepancy implies that some other technique is needed to test the accuracy of current methods. One of the solutions proposed is measuring SFR using core-collapse supernovae (CC SNe) rate [9].

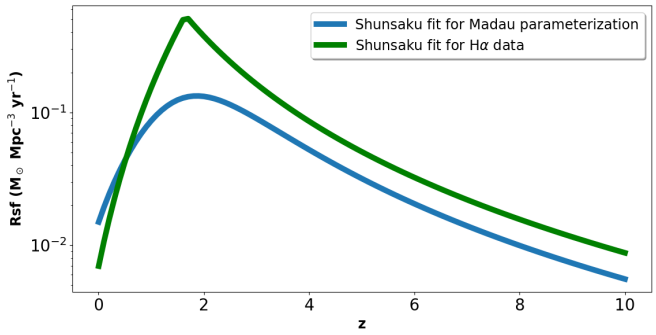

FIG. 1: Star Formation Rate

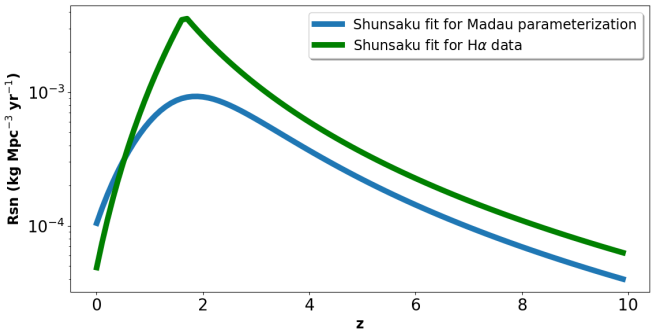

FIG. 2: CC SNe Rate

It is based on the assumption that the universe is in equilibrium, i.e., the star formation rate is equal to the rate of death of stars. Since the mass range of stars ending with CC SNe is known, the fraction of star-deaths resulting in CC SNe can be calculated. This information enables us to estimate SFR using the measurement of CC SNe rate. However, its measurement, using the methods based on the electromagnetic spectrum, has its challenges. In Horiuchi, it is mentioned that a significant fraction of supernova can not be detected due to dust attenuation (the most probable value of the fraction is 0.19, and upper and lower bars are 0.13 and 0.28 respectively). So, in this paper, it is proposed to measure CC SNe rate using DSNB, which is ultimately used to infer the SFR. In the next section, this methodology is explained in detail.

DSNB AS A PROBE FOR SFR MEASUREMENT

The Diffuse Supernova Neutrino Background (DSNB) is the flux of neutrinos and antineutrinos emitted by all CC SNe in the causally-reachable universe; it will appear isotropic and time-independent in feasible observations. The equation governing the DSNB flux spectrum at Earth [4]:

$$\frac{d\phi}{dE_{\rm d}} = \int_0^\infty \Big[(1+z)\phi[E_{\rm d}(1+z)]\Big]\Big[R_{SN}(z)\Big]\left[c\left|\frac{dt}{dz}\right|dz\right] \tag{5}$$

In the above equation, $\frac{d\phi}{dE_{\rm d}}$ represents the total number of neutrinos arrived per unit time of detection per unit energy of detection per unit area of detector, $\phi[E_{\rm d}(1+z)]$ represents number of neutrinos detected for a single CC SNe per unit emitted energy and $R_{SN}(z)$ represents the evolving CC SNe rate. For the derivation of the above equation, it is assumed that neutrinos are massless (i.e., $ds^2 = 0$ for neutrinos).

The neutrino spectra emitted from a CC SNe are not understood well enough and, so the effective observable spectra is used. For $\bar{\nu}_e$ (the type of neutrinos which are detected in detectors), the effective time-integrated spectrum is assumed to be of the Fermi-Dirac form [4]:

$$\phi(E_{\rm d}(1+z)) = \frac{E_{\phi_e(tot)}}{6}\frac{120}{7\pi^4}\frac{E_d^2(1+z)^2}{T^4}\frac{1}{e^{E_d(1+z)/T}+1} \tag{6}$$

The total energy emitted in a CC SNe ($E_{\phi_e(tot)}$) is not fixed from theory but will be determined from different experiments. For SN 1987A, it is determined to be $\sim 5\times10^{52}$ erg [4], which is the value used in this paper. In Abe et al., it is speculated that 70 percent of CC SNe emits neutrinos at the energy corresponding to the neutrino temperature of 4 MeV while rest 30 percent at 8 MeV. Note that, for the work of this paper, the properties of CC SNe (such as temperature and total energy of emitted neutrinos) are assumed to be constant and redshift independent for different supernova.

Ratio of R_{SF} and R_{SN} is derived $143M_\odot$, assuming Salpeter IMF and that stars between masses 8 to 50 times solar mass result in CC SNe:

$$R_{SN}(z) = \frac{R_{SF}}{143M_\odot} \tag{7}$$

Using Friemann equation, $\frac{dt}{dz}$ comes out to be:

$$\frac{dt}{dz} = -\frac{1}{H_o}\frac{1}{1+z}\frac{1}{\sqrt{\Omega_m(1+z)^3+\Omega_\Lambda+\Omega_r(1+z)^4}} \tag{8}$$

In figure 2, CC SNe rate, on assumption of SFR, according to Madua parameterization (UV+IR data) and according to H_α data, is shown. The corresponding neutrino arrival flux $\frac{d\phi}{dE_{\rm d}}$ is shown in figure 3. To do further analysis, i.e., obtain the positron detection spectrum and perform likelihood test, specifications of twin detectors of Hyper-Kamiokande Experiment, is assumed. In the next section, the Hyper-Kamiokande Experiment is discussed in detail.

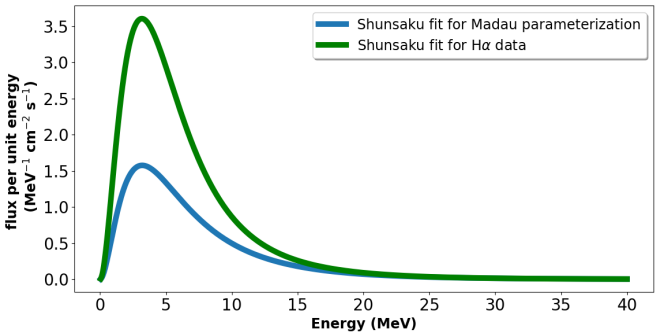

FIG. 3: Neutrino Arrival spectrum

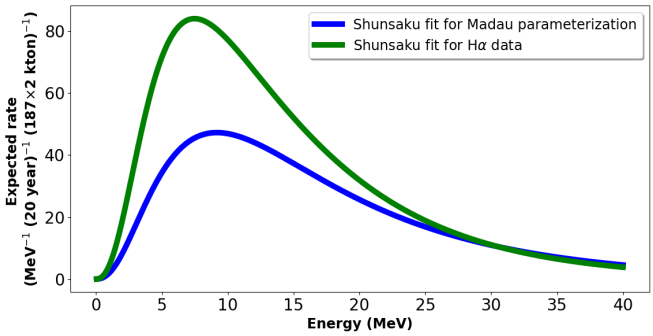

FIG. 4: Expected positron spectrum in 20 years of measurement

DSNB DETECTION AT HYPER-KAMIOKANDE

Hyper-Kamiokande (Hyper-K) is a next-generation underground water Cherenkov detector, based on the Super-Kamiokande experiment. Positrons (e^+), formed in inverse beta decay ($\bar{\nu}_e + p \rightarrow e^+ + n$), are detected in the reactor. The strategy of the future Hyper-K experiment is to build two identical water Cherenkov detectors in stage with 260 kton of purified water per detector. Since, the first detector, proposed to build, has a fiducial volume of 187 kton, in this paper all the analysis is done assuming the availability of 187×2 kton of water. With 0.1 percent gadolinium dissolved in the water, capture efficiency is given to be 90 percent [1].

Equation relating positron detection flux at the detector to neutrino arrival flux [4]:

$$\frac{(dN_{e^+})_{\rm d}}{dE_{e^+}dt_{\rm d}} = \frac{d\phi}{dE_{\rm d}}\sigma(E_{\rm d})N_p \tag{9}$$

In above equation, $\sigma(E_{\rm d})$ is cross section area of proton for reaction with neutrino as a function of neutrino energy and N_p is number of protons in detector. To calculate number of protons, it is assumed that only protons of hydrogen atoms in water molecule can participate in inverse beta decay. Therefore number of protons is twice the number of water molecules in the detector. Neutrino energy ($E_{\rm d}$) is related with energy of positron (E_{e^+}) formed as $E_{\rm d} \approx E_{e^+} + 1.3MeV$.
$\sigma(E_{\rm d})$ is given as:

$$\sigma(E_{\rm d}) = \left[0.0952 \times 10^{-42}\ {\rm cm}^2\ (E_{\rm d} - 1.3\ {\rm MeV})^2\right] \times (1 - 7E_{\rm d}/M_p) \tag{10}$$

where M_p is proton mass in natural units.

Thus, positron detection rate is only a function of detected positron energy and assumed star formation rate. If we assume a star formation rate, then a positron detection spectrum will be obtained by plugging in the assumed R_{SF} in equation 7. Therefore, a comparison of the experimentally obtained spectrum with the predicted spectrum can verify whether the assumed SFR is correct or not. Positron spectra detected in 20 years when both the Hyper-Kamiokande detectors are operational is shown in figure 4.

Background noises at Hyper-Kamiokande

As can be seen in figure 4, the difference in positron spectrum is sizeable from ∼1 MeV to 25 MeV. There are mainly three kinds of background in this energy range.

- Invisible muon background - charged-current interactions of atmospheric muon neutrinos produce muons below Cherenkov threshold (so invisible) whose decay produces electrons
- Low energy atmospheric neutrinos - neutrinos produced by cosmic-ray interactions in the atmosphere
- Neutrinos from nuclear reactors

Detection Threshold

Below 10 MeV, neutrinos from the nearby nuclear reactors are several order of magnitude larger than the actual signal at Hyper-K. There is a resolution tail of the reactor neutrinos above 10 MeV too, but in Abe et al., it is assumed that analysis with a lower energy threshold of ∼10 MeV is possible. Therefore, for the analysis done in this paper, the lower cut for neutrino detection is assumed to be 10 MeV, and above this, the reactor neutrino background is assumed to be controlled while doing the analysis.

In figure 5, positron spectra, along with the backgrounds, are shown. For the analysis done in this paper, spectra between 10 and 25 MeV is considered.

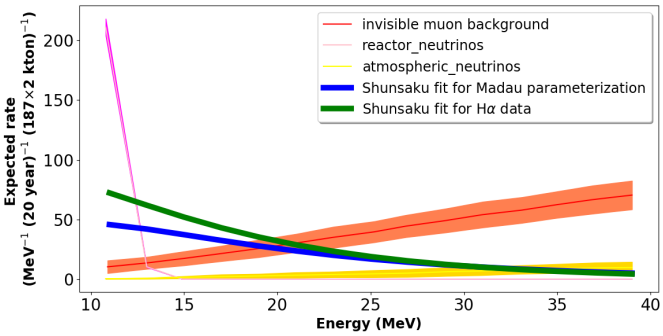

FIG. 5: Background noise above 10 MeV

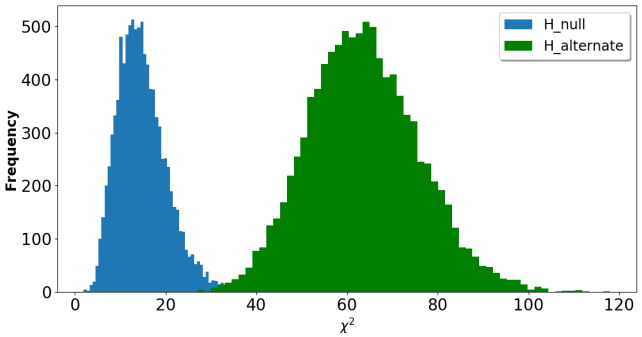

FIG. 6: χ^2 distribution without background

SFR VERIFICATION USING DSNB

The purpose of the analysis done in this paper is to check whether the discrepancy in SFR inferred using two different probe-systems (UV + IR and Hα) can be resolved using DSNB. χ^2 test is used for the same.

In the χ^2 test, a hypothesis is assumed to be correct and is called the null hypothesis. Alternate hypotheses are all other hypotheses being tested against this hypothesis. Experimental data is generated using Monte-Carlo Simulation. χ^2 is calculated using equation 11. Consequently, several χ^2 distribution will be obtained using the predicted data for different hypotheses. Depending on the separation of χ^2 distribution corresponding to null and an alternative hypothesis, it can be predicted whether the alternate hypothesis can be rejected using the actual experimental data or not.

$$\chi^2 = -2\ \ln L \tag{11}$$

where L is likelihood.

Based on the advantages of UV and IR probe over Hα, the Shunsaku fit for UV+IR data is assumed to be the defining equation for co-moving star formation rate, i.e., it is the null-hypothesis. Consequently, the alternate hypothesis is the one in which the Shunsaku fit for Hα data is assumed to be the defining equation.

χ^2 test without background

For a start, it is assumed that there is no noise in the detector. Experimental data is generated from Poisson distribution about the positron spectrum corresponding to the null hypothesis, and predicted data is positron spectrum corresponding to the hypotheses. χ^2 is given by equation 12. Its distribution is shown in figure 6. As can be seen in the figure, they are well separated and can be easily excluded.

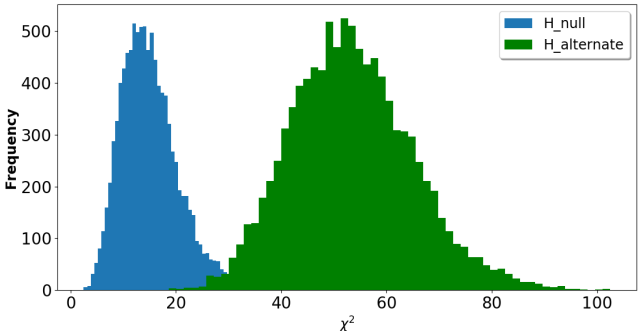

FIG. 7: χ^2 distribution with known background

$$\chi^2 = \sum \frac{(X_{expt} - X_{pred})^2}{X_{pred}} \tag{12}$$

where X_{expt} and X_{pred} stands for experimental and predicted data respectively.

χ^2 test with known background

In the next test, the background is added, but it is assumed to be known, i.e., there is no uncertainty associated with the background. Experimental data is generated from Poisson distribution about the sum of mean background and positron spectrum corresponding to the null hypothesis, and predicted data is the sum of mean background and positron spectrum corresponding to the hypotheses. χ^2 is given by equation 12. As can be seen in figure 7, results are practically the same, i.e., they are well separated and can be easily excluded.

χ^2 test with uncertain background

Generation of experimental data

100 spectra of expected background are obtained from Gaussian distribution about mean background. It is added to the positron spectrum corresponding to null spectrum, to obtain 100 expected net-spectra. Corresponding to each expected net-spectra, 100 spectra are generated using Poisson distribution. Consequently, 10000 sets of experimental data are obtained.

Generation of predicted data

The predicted data is not assumed to be the sum of mean background and positron spectrum corresponding to the null hypotheses because according to Bohm and Zech, the replacement of the nuisance parameter (background in our case) by its estimate leads to an illegitimate reduction of the error limits whenever the nuisance parameter and the interesting parameter (net-spectra in our case) are correlated. Therefore, Profile likelihood is used for the generation of the predicted data.

In Profile likelihood, χ^2 values are calculated by comparing the experimental data with sum of an assumed background and positron spectrum corresponding to the hypotheses. For a hypothesis, the background corresponding to minimum χ^2 value is assumed to be the experimental background. The predicted value used for χ^2 test is the sum of this background and positron spectrum corresponding to the hypotheses. Note that due to the inclusion of uncertainty on background, χ^2 will contain Gaussian prior too (equation 13). Result is shown in figure 8. As can be seen from the figure, there is a significant overlap between both the χ^2 distribution. The alternative hypothesis can be excluded at a level of 81.77 percent, which is not an adequate number.

$$\chi^2 = \sum \left[\frac{(X_{expt} - X_{pred})^2}{X_{pred}} + \frac{(bg_{expt} - bg_{mean})^2}{bg^2_{unc}} \right] \quad (13)$$

where bg_{expt}, bg_{mean} and bg_{unc} stands for experimental background, mean background and uncertainty in background respectively.

BACKGROUND-UNCERTAINTIES REDUCTION

The muon flux, used in this work, is obtained by Abe et al. (2018) using the muon simulation code (MUSIC). They have assumed the same rock type as used in Abe et al. (2010) due to the similarity in the geology of two sites. Since muon flux is dependent on the type of rock,

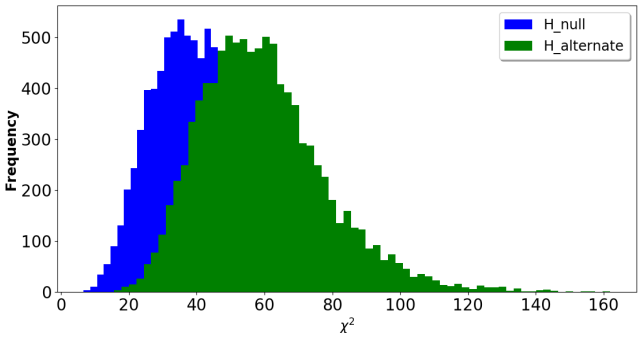

FIG. 8: χ^2 distribution with uncertain background

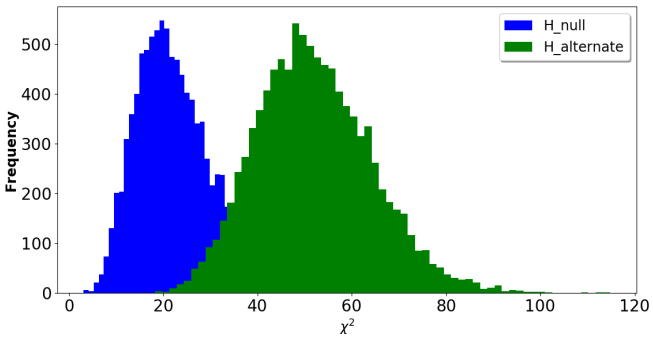

FIG. 9: χ^2 distribution with half uncertain background

an uncertainty of $\pm 20\%$ has been assumed for muon flux. Therefore, improvement in understanding of rocks at the site would improve the knowledge of backgrounds and reduce the uncertainty in its value.

As seen in the previous section, with current technological limitation and knowledge of background noises, resolution of discrepancy in SFR between UV+IR and Hα probe is not possible. However, with improved knowledge of background noises and tighter limits on the uncertainty, the results are improved. Result obtained on repeating the χ^2 test with the assumption that uncertainty in the total background is half the current value, is shown in figure 9. The χ^2 distribution is separated enough to exclude the SFR obtained using Hα measurements at a 99 percent confidence level.

CONCLUSIONS

It has been shown in this paper that DSNB measurement can play a critical role in the resolution of SFR measured from different probes. At present, the knowledge of parameters used to characterize neutrino emission from CC SNe is uncertain. These parameters can be better determined with an improved observation of core-collapse supernova events happening in the

nearby universe [3]. Changes in the value of these parameters will affect the results shown in this paper. Nevertheless, one deduction that remains unchanged is that as the detectors become more significant in volume and the noise rejection or determination capability improves, DSNB measurement will be able to put stringent limits on the parameters involved in the defining equation of co-moving SFR. The improved determination of the SFR equation, in turn, will improve our understanding of cosmic noon.

* Electronic address: 160100097@iitb.ac.in
† Electronic address: rentala@phy.iitb.ac.in

[1] K. Abe et al. Hyper-Kamiokande Design Report. 2018.

[2] S. Abe, S. Enomoto, K. Furuno, Y. Gando, H. Ikeda, K. Inoue, Y. Kibe, Y. Kishimoto, M. Koga, Y. Minekawa, T. Mitsui, K. Nakajima, K. Nakajima, K. Nakamura, M. Nakamura, I. Shimizu, Y. Shimizu, J. Shirai, F. Suekane, A. Suzuki, Y. Takemoto, K. Tamae, A. Terashima, H. Watanabe, E. Yonezawa, S. Yoshida, A. Kozlov, H. Murayama, J. Busenitz, T. Classen, C. Grant, G. Keefer, D. S. Leonard, D. McKee, A. Piepke, T. I. Banks, T. Bloxham, J. A. Detwiler, S. J. Freedman, B. K. Fujikawa, F. Gray, E. Guardincerri, L. Hsu, K. Ichimura, R. Kadel, C. Lendvai, K. B. Luk, T. O'Donnell, H. M. Steiner, L. A. Winslow, D. A. Dwyer, C. Jillings, C. Mauger, R. D. McKeown, P. Vogel, C. Zhang, B. E. Berger, C. E. Lane, J. Maricic, T. Miletic, M. Batygov, J. G. Learned, S. Matsuno, S. Pakvasa, J. Foster, G. A. Horton-Smith, A. Tang, S. Dazeley, K. E. Downum, G. Gratta, K. Tolich, W. Bugg, Y. Efremenko, Y. Kamyshkov, O. Perevozchikov, H. J. Karwowski, D. M. Markoff, W. Tornow, K. M. Heeger, F. Piquemal, J. S. Ricol, and M. P. Decowski. Production of radioactive isotopes through cosmic muon spallation in kamland. *Phys. Rev. C*, 81:025807, Feb 2010. doi: 10.1103/PhysRevC.81.025807. URL `https://link.aps.org/doi/10.1103/PhysRevC.81.025807`.

[3] Shin'ichiro Ando, John F. Beacom, and Hasan Yüksel. Detection of neutrinos from supernovae in nearby galaxies. *Phys. Rev. Lett.*, 95:171101, Oct 2005. doi: 10.1103/PhysRevLett.95.171101. URL `https://link.aps.org/doi/10.1103/PhysRevLett.95.171101`.

[4] John F. Beacom. The Diffuse Supernova Neutrino Background. *Ann. Rev. Nucl. Part. Sci.*, 60:439–462, 2010. doi: 10.1146/annurev.nucl.010909.083331.

[5] Gerhard Bohm and Gnter Zech. Introduction to statistics and data analysis for physicists. 01 2010.

[6] Shunsaku Horiuchi. Supernova rates and star formation rates. `https://www.cis.fukuoka-u.ac.jp/~kkotake/MMCOCOS_prog/horiuchi_MMCOCOS.pdf`, 2013.

[7] Shunsaku Horiuchi, John F. Beacom, and Eli Dwek. The Diffuse Supernova Neutrino Background is detectable in Super-Kamiokande. *Phys. Rev.*, D79:083013, 2009. doi: 10.1103/PhysRevD.79.083013.

[8] Janice C. Lee et al. Comparison of H-alpha and UV Star Formation Rates in the Local Volume: Systematic Discrepancies for Dwarf Galaxies. *Astrophys. J.*, 706: 599–613, 2009. doi: 10.1088/0004-637X/706/1/599.

[9] Piero Madau and Mark Dickinson. Cosmic star-formation history. *Annual Review of Astronomy and Astrophysics*, 52:415–486, 2014.

[10] Valeria Politino. The history of star-formation in galaxies. Thesis; UNIVERSIT DEGLI STUDI DI PADOVA.

[11] Hyunjin Shim, James Colbert, Harry Teplitz, Alaina Henry, Mattew Malkan, Patrick McCarthy, and Lin Yan. GLOBAL STAR FORMATION RATE DENSITY OVER 0.7 z 1.9. *The Astrophysical Journal*, 696 (1):785–796, apr 2009. doi: 10.1088/0004-637x/696/1/785. URL `https://doi.org/10.1088%2F0004-637x%2F696%2F1%2F785`.

[12] Ken-ichi Tadaki, Tadayuki Kodama, Yusei Koyama, Masao Hayashi, Ichi Tanaka, and Chihiro Tokoku. Cosmic Star Formation Activity at z=2.2 Probed by H-alpha Emission Line Galaxies. *Publ. Astron. Soc. Jap.*, 63:437, 2011. doi: 10.1093/pasj/63.sp2.S437.

[13] Rachel Theios. The Universe at Cosmic Noon. `https://www.youtube.com/watch?v=zAKUtROZAy0`, 2019.

[14] Mark Whittle. STAR FORMATION STARBURST GALAXIES. `http://people.virginia.edu/~dmw8f/astr5630/Topic11/Lecture_11.html#sec4`, 2011.